Journal of Magnetism and Magnetic Materials 475 (2019) 620–626

Contents lists available at ScienceDirect

Journal of Magnetism and Magnetic Materials

journal homepage: www.elsevier.com/locate/jmmm

Research articles

Study of anisotropy of magnetic noise, generated by magnetic particles in geomagnetic field

M.A. Polikarpov[a,*], M.N. Ustinin[b], S.D. Rykunov[b], A.Y. Yurenya[a,c], S.P. Naurzakov[a], A.P. Grebenkin[a], V.Y. Panchenko[a,c]

[a] National Research Center "Kurchatov Institute", Moscow, Russia
[b] Keldysh Institute of Applied Mathematics, Moscow, Russia
[c] Faculty of Physics, Lomonosov Moscow State University, Moscow, Russia

ARTICLE INFO

Keywords:
Magnetic nanoparticles
Ferrofluid
Magnetoencephalography
Spectral analysis
Functional tomography

ABSTRACT

Any existing method of visualization of magnetic nanoparticles in biological objects provides for imposing of an external magnetic field on the object under study. The field can considerably change the space distribution and properties of the nanomagnetic ensemble under study. In our work a SQUID-based magnetoencephalography device was used for the measurement of a magnetic noise generated by superparamagnetic nanoparticles based ferrofluid in the stationary standing vial without imposing of an external magnetic field. It was demonstrated that the ferrofluid generates spontaneous magnetic fields sufficient for its localization inside the experimental setup. Besides it was revealed that the spontaneous magnetic fields at certain frequencies have a strong spatial anisotropy. The detected effect can essentially increase the spatial resolution of the proposed method of visualization of magnetic nanoparticles in biological objects without using the external magnetic field.

1. Introduction

The clinical application of magnetic carriers is restrained by the lack of methods for visualization of the spatial distribution of the carriers and the products of their biodegradation within the living organism. The visualization is usually realized using magnetic particles imaging (MPI) [1], magnetic resonance imaging (MRI) [2] or magnetorelaxometry (MRX) [3] methods. A tomograph based on these techniques requires a group of sensors that are distributed in space near the living object under study. The sensors generate electrical signals proportional to the magnetic field, which is created by the magnetic carriers at the sensors locations. Magnetic carriers usually consist of superparamagnetic iron oxide nanoparticles. Their average magnetization in the absence of an external magnetic field is zero. Therefore, in all above-mentioned methods it is necessary to impose on the object magnetic fields with induction from 10^{-3} to several Tesla.

A significant drawback of this method of visualization is the fact that magnetic fields applied to the object in the process of measurement not only magnetize superparamagnetic nanoparticles, but also lead to a change in their distribution in space. The size of a human body cell is about thousand times greater than the size of a superparamagnetic nanoparticle. Therefore, the particles in a living cell retain considerable freedom of movement in a quasi-liquid intracellular medium [4], including the motion under the action of an external magnetic field [5–7].

Two mechanisms are known for restructuring ensembles of magnetic nanoparticles in an intracellular medium under the action of a magnetic field. The first is related to the directed motion of magnetic nanoparticles in an inhomogeneous magnetic field to the region where this field is larger. The second takes place in a homogeneous magnetic field and is related to the fact that if two superparamagnetic particles lie on the same magnetic line, they attract one another, and if they are parallel to these lines, they repel each other [8]. As a result, under the influence of an external magnetic field, the magnetic nanoparticles can cluster or align themselves in chains oriented along lines of the magnetic field [9,10].

The above readjustment of magnetic particles, when a measuring magnetic field is imposed on them, depends on the magnitude of this field, the duration of its imposition [11] and on the viscosity of the intracellular medium. It turns out that such a readjustment of superparamagnetic nanoparticles in living cells occurs even in the Earth's magnetic field, which is two orders of magnitude smaller than the minimum magnetic fields used in the above-mentioned tomographic methods [12]. In view of the permanent residence of living organisms in the geomagnetic field, this field proves to be enough to magnetize

* Corresponding author.
E-mail address: polikarpov_imp@mail.ru (M.A. Polikarpov).

https://doi.org/10.1016/j.jmmm.2018.12.011
Received 24 June 2018; Received in revised form 3 December 2018; Accepted 4 December 2018
Available online 05 December 2018
0304-8853/

located in these organisms biogenic superparamagnetic nanoparticles [13]. Pulsed measuring magnetic fields destroy this naturally ordered nanomagnetic state [14]. The ability of the geomagnetic field to magnetize superparamagnetic nanoparticles in living cells opens the possibility for their visualization in a natural state that is not distorted by additional external magnetic fields.

The possibility of the visualization of magnetic nanoparticles in the samples subjected to the motion in the geomagnetic field instead of the pre-magnetization was demonstrated for the first time in Ref. [15] using the high sensitivity SQUID magnetoencephalography (MEG) device. The possibility of the detection of magnetic nanoparticles in the ferrofluid using MEG device without pre-magnetization and even without forced movement of the sample was first demonstrated in Ref. [16]. The authors of the last paper found that the frequency spectrum of the MEG data with the ferrofluid sample was greater than the baseline sensor noise. The comparison between spatial contour maps of the frequency data measured without the sample and with the sample showed a distinct increase in frequency power just at the location of the sample. In Ref. [17] a single channel SQUID based system was used for the noise measurements from nanoparticles immersed in water, gel and solid gypsum matrix in the absence of any external excitation. It should be noted that in the last two papers the mechanism of generation of the observed magnetic noise was not determined, although the discussion mentioned Neel and Brownian mechanisms of its possible generation.

7-Channel SQUID based MEG device was used in Ref. [18] for the determination of the source of the magnetic noise generated by ferrofluid in the stationary standing vial. It was found that the movement of nanoparticles at free surface of the ferrofluid generates the magnetic noise sufficient for determination of location of the vial in the experimental setup. This discovery allows us to offer a new approach for visualization of the spatial distribution of superparamagnetic nanoparticles within the living organism. In this approach the geomagnetic field orients magnetic nanoparticles in one direction. The change in magnetic flux from these oriented magnetic particles occurs because of their natural fluctuation movement. The sources of such movement in the living body can be breath, heartbeat or Brownian motion of nanoparticles in the cytoplasm of cells. The principal possibility of such 3D imaging of magnetic nanoparticles in the ferrofluid using the 7-channel SQUIDs based magnetoencephalography (MEG) device without pre-magnetization and forced movement of the sample was demonstrated in Ref. [18]. The spatial distribution of elementary magnetic sources was reconstructed by the method of frequency-pattern analysis of multichannel time series [19–21]. This method decomposes the multichannel signal into the large set of elementary oscillations, which can be localized individually, providing the functional tomogram of the system. The localization of ferrofluid was performed based on the analysis of quasi-random time series in two cases of oscillation source. One of them was infrasound from the outer urban noise, and another one was the human heartbeat. The purpose of the present work was to study an angular distribution of the magnetic noise, generated by such oscillating magnetic nanoparticles in geomagnetic field.

2. Materials and methods

2.1. Samples

The mixture of 2 g $FeCl_2{\cdot}4H_2O$ and 5,42 g of $FeCl_3{\cdot}6H_2O$ (Fe^{2+} and Fe^{3+} mole ratio = 1:2) was placed in a flask and dissolved in 10 ml of deionized water. The resulting solution was stirred for 5 min with magnetic stirrer and 250 ml of 0.7 M NH_4OH solution was added with continuous stirring for 30 min at room temperature. The resulting suspension was precipitated on the permanent magnet and the supernatant was poured. Then, the precipitate was washed 4 times with aqueous solution of citrate (20 mg/ml) each time the suspension was stirred for 10 min and precipitated. After that the particles were collected and resuspended in deionized water. The concentration of the nanoparticles solution obtained was 2 mg/ml. The mean size of the resulting nanoparticles 10–12 nm was evaluated by the Mossbauer spectroscopy method.

For obtaining gelatinous samples 0,8 g of agarose was dissolved in 5 ml distilled water by heating to 95 °C while stirring. The agarose solution was cooled to 50 °C and then added to 35 ml of nanoparticles solution at room temperature with continuous intensive stirring. Then the resulting solution was at once poured into 40 ml plastic vial. Total agarose gel concentration achieved was 2%.

2.2. Multichannel magnetic measurements

The measurements were carried out at previously described [18] 7-channel MEG device, designed for non-contact recording of a magnetic encephalogram of a human brain. The planar set of sensors has a hexagonal structure and includes 7 second-order SQUID gradiometers. One gradiometer is located in the center of the hexagon. The distances between the gradiometers are 30 mm. The sensors demonstrate an intrinsic noise level lower than 5 fT/√Hz. The MEG device was placed inside a thick-walled aluminum camera, designed for shielding from an alternating electromagnetic field. No shielding from static magnetic field was used.

2.3. Numerical modeling

The system under study is considered to be a set of many elementary permanent magnets, which are produced in ferrofluid by geomagnetic field. These magnets are oriented in the direction of the Earth magnetic field (in Moscow it is Declination ≈ 11°, Inclination ≈ 71°). The motion of each constant magnet is produced by the minor oscillations in ferrofluid from the urban noise or from the human heartbeat [18].

The magnetic field of the permanent magnet is modelled by the field of magnetic dipole – the coil with current I, radius a and direction $\boldsymbol{Q}$, located in $\mathbf{r}$. The magnetic induction B_k can be calculated [24] for the sensor number k with location $\boldsymbol{r}_k$ and direction $\boldsymbol{n}_k$:

$$B_k = \frac{\mu_0 I}{\pi\alpha^2\beta}\left(\left(\frac{z}{d}\,(\alpha^2\,(E(\gamma^2)-K(\gamma^2))-2adE(\gamma^2))\boldsymbol{e_d} + (\alpha^2(K(\gamma^2)-E(\gamma^2))+(2a^2+2ad)E(\gamma^2))\boldsymbol{Q}\right),\boldsymbol{n_k}\right) \quad (1)$$

where

$\alpha^2 = a^2 + d^2 + z^2 - 2da;\ \beta^2 = a^2 + d^2 + z^2 + 2da;\ \gamma^2 = 1 - \frac{\alpha^2}{\beta^2};$

$\boldsymbol{r}_a = \boldsymbol{r}_k - \boldsymbol{r};\ z = (\boldsymbol{r}_a, \boldsymbol{Q});\ \boldsymbol{d} = \boldsymbol{r}_a - z\boldsymbol{Q};\ d = |\boldsymbol{d}|;\ \boldsymbol{e_d} = \frac{\boldsymbol{d}}{|d|};\ |\boldsymbol{n}_k| = 1;$

$K(\gamma^2)$ – elliptic integral of the first kind, $E(\gamma^2)$ – elliptic integral of the second kind.

Let us consider the set of 900 × 900 sensors, uniformly covering the plane $9 \times 9\ \mathrm{cm}^2$, which includes the lowest set of sensors in our experiment. All sensors have vertical orientation $\boldsymbol{n}_k = (0, 0, 1)$. Calculating B_k for each sensor, it is possible to obtain the field map (see Fig. 1a). The movement of the magnet in the direction X is modelled by adding small oscillating part $x_d \sin(2\pi\nu t)$ to the $\boldsymbol{r}_x$ and calculating (1) for all model sensors, thus obtaining the set of functions $B_k(t) = B_{0k} + B_{dk}(t)$. Further conclusions are based on the fact, that SQUID-sensors cannot register the constant magnetic field. To model the experimental data, we estimate B_{0k} for each channel as $B_{0k} = \frac{1}{N}\sum_{i=1}^{N} B_k(t_i)$, where t_i uniformly cover the period of the frequency ν. Then B_{0k} is subtracted from $B_k(t)$, giving the oscillating field $B_{dk}(t)$ (see Fig. 1b). This field is similar to the field of the oscillating magnetic dipole with fixed location $\mathbf{r}$ and direction $(1, 0, 0)$ (direction corresponds to mechanical movement), see Fig. 1c. Note, that field at Fig. 1b is calculated for the moment of maximal deviation x_d. The current of magnetic dipole at Fig. 1c is I. For the moment of minimal deviation $-x_d$, signs of the field will flip to opposite, so the current of magnetic

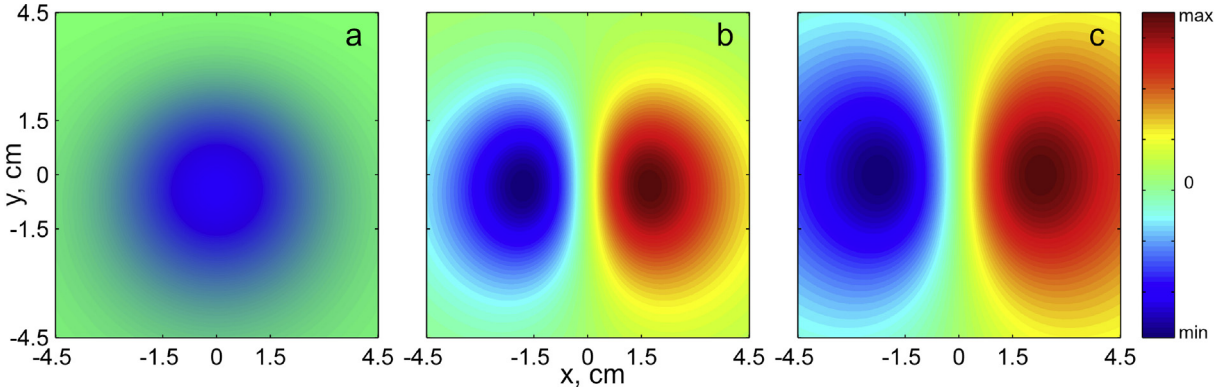

Fig. 1. Model magnetic fields, calculated in the plane of the lowest set of sensors: a – field map of the permanent magnet, located in (0, 0, −4.5 cm) and oriented along the Earth magnetic field; **b** – field map of this magnet, oscillating along the X axis with amplitude 0.2 cm. Field map is shown with subtracted average B_{0k} at each point; **c** – field map of the oscillating magnetic dipole with fixed location (0, 0, −4.5 cm) and direction along the X axis. All fields are shown in relative units (see Legend), because in our approach we analyze normalized field patterns.

dipole will be $-I$.

It can be concluded, that it is possible to use static magnetic dipole with alternating current as a model for the description of mechanical movement of the magnet, formed in ferrofluid by the geomagnetic field. Physical reason for such modeling lays in the fact, that SQUID sensors register not the field of this magnet, but only the changes of the field.

As follows from this simulation, the magnetic field of the moving magnet is generally similar to the field of static alternating dipole, while there are some differences (see Fig. 1b and c). Let us assume, that we are going to estimate the movement parameters by the fitting of the field Fig. 1c to the field Fig. 1b. One can see, that the coordinates x and y of the central point, determined as the middle of the distance between the maximum and minimum of the fields (red and blue bulk), will be estimated correctly. Coordinates x and y of this position are the same at Fig. 1b and c. The direction of the movement will be also estimated correctly. This direction corresponds to the line, connecting the maximum and the minimum of the fields. At the same time, for z-coordinate we can obtain only qualitative goodness of fit, because the dipole at the Fig. 1b is much more compact than the dipole at the Fig. 1c. The dipole at the Fig. 1b can contain components of higher orders (quadruple and higher). In this study we use Eq. (1) for the approximate description of the ferrofluid motion. More precise description of the field changes, registered by the SQUID sensors, can be written as

$$B_k^{var} = (\nabla B_k, \boldsymbol{u}(t)) \tag{2}$$

where $\boldsymbol{u}(t)$ is a vector function of the time, describing small motion of the magnet, and the gradient of B_k is calculated with respect to the variable $\mathbf{r}$ – initial location of the magnet.

We are going to use Eq. (2) to solve the inverse problem in our further studies.

2.4. Data analysis

The method of data analysis is based on Fourier transform and coherence analysis. It was developed in Ref. [19] to study various complex systems and was applied to investigate the human brain spontaneous activity [20,21]. Magnetic fields were recorded using a MEG system, consisting of K sensors (channels), which provided the set of experimental vectors $\{\mathrm{b}_k\}$, $k = 1, \ldots, K$. This approach discretely samples sets of continuous functions $\{\widetilde{B}_k(t)\}$ – magnetic inductions in K channels.

The multichannel Fourier transform calculates a set of spectra:

$$a_{nk} = \frac{2}{T}\int_0^T \widetilde{B}_k(t)\cos(2\pi\nu_n t)dt,$$
$$b_{nk} = \frac{2}{T}\int_0^T \widetilde{B}_k(t)\sin(2\pi\nu_n t)dt, \tag{3}$$

where a_{nk}, b_{nk} are Fourier coefficients for the frequency ν_n in the channel number k, and $n = 1, \ldots N$, $N = \nu_{max}T$, where ν_{max} is the highest desirable frequency. The coefficient for $n = 0$ is not considered, because the constant field component has no meaning in SQUID measurements. Given high sampling frequency (1000 Hz), vectors $\{\mathbf{b}_k\}$ represent continuous functions $\{\widetilde{B}_k(t)\}$ with sufficient accuracy, such that integrals (3) can be effectively calculated using discrete Fourier transform [22].

To reveal the detailed frequency structure of the system, all spectra were calculated for the whole time of registration T. The frequency resolution is equal to $\Delta\nu = \nu_n - \nu_{n-1} = 1/T$, so it is determined by the recording time. In this study, all time series were measured for 20 min, thus providing frequency resolution 0.000833 Hz.

In order to study the system in frequency space, we restored multichannel signal at every frequency ν_n in all channels and analyzed the functions obtained:

$$B_{nk}(t) = \rho_{nk}\sin(2\pi\nu_n t + \varphi_{nk}) \tag{4}$$

where $\rho_{nk} = \sqrt{a_{nk}^2 + b_{nk}^2}$, $\varphi_{nk} = \mathrm{atan2}(a_{nk}, b_{nk})$, a_{nk}, b_{nk} are Fourier coefficients, found in (1), $t \in [0, T_{\nu_n}]$, $T_{\nu_n} = 1/\nu_n$ is the period of this frequency.

If $\varphi_{nk} = \varphi_n$, then formula (4) describes a coherent multichannel oscillation and can be written as

$$B_{nk}(t) = \rho_n\hat{\rho}_{nk}\sin(2\pi\nu_n t + \varphi_n) \tag{5}$$

where $\rho_n = \sqrt{\sum_{k=1}^{K}\rho_{nk}^2}$ is the amplitude, and $\hat{\rho}_{nk} = \rho_{nk}/\rho_n$ is the normalized pattern of oscillation. The normalized pattern $\hat{\rho}_{nk}$ makes it possible to determine the spatial structure of the source from the inverse problem solution, and this structure is constant throughout the entire period of the oscillation. The time course of the field is determined by the function $\rho_n\sin(2\pi\nu_n t + \varphi_n)$ which is common for all channels, i.e. this source is oscillating as a whole at the frequency ν_n. In order to estimate general spectral features of various experimental data, we use the sum of powers in all channels:

$$\mathrm{Power}(\nu_n) = \sum_{k=1}^{K}\rho_{nk}^2 \tag{6}$$

where ρ_{nk} is calculated in (4).

The theoretical foundations for the reconstruction of static functional entities, or sources, have been developed in Ref. [19]. This

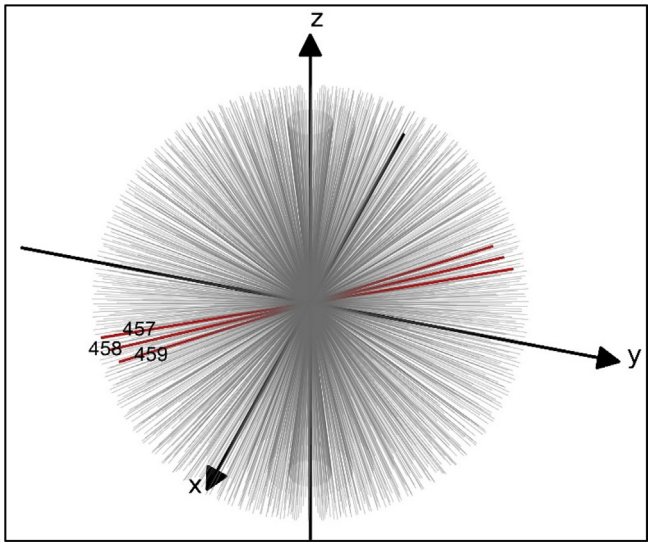

Fig. 2. The set of 931 trial directions, uniformly covering the sphere (gray). Three dominant directions (red) revealed in experiment with magnetic noise, see Fig. 3. (For interpretation of the references to color in this figure legend, the reader is referred to the web version of this article.)

reconstruction is based on detailed frequency analysis and extraction of the frequencies, having high coherence and similar patterns.

The algorithm of massive frequency-pattern analysis was formulated as follows:

1. Discrete Fourier Transform of the multichannel signal for the whole recording time T.
2. Inverse Fourier Transform – restoration of the signal at each frequency.
3. If the coherence at the particular frequency is high, then use the pattern and frequency as elementary coherent oscillation (5).
4. If the restored signal consists of several phase-shifted coherent oscillations, then extract those oscillations by the Independent Component Analysis [23].

After the fourth step of this analysis, the initial multichannel signal is represented as a sum of elementary coherent oscillations:

$$B_k(t) \cong \sum_{n=1}^{N} \sum_{m=1}^{M} D_{mn} \hat{\rho}_{mnk} \sin(2\pi\nu_n t + \varphi_{mn}),$$
$$\nu_n = n/T, \quad N = \nu_{max} T, \tag{7}$$

where M is maximal number of coherent oscillations, extracted at the frequency ν_n.

Each elementary oscillation is characterized by frequency ν_n, phase φ_{mn}, amplitude D_{mn}, normalized pattern $\hat{\rho}_{mnk}$ and is produced by the functional entity having a constant spatial structure.

The method of functional tomography reconstructs the electrical functional structure of the system from the analysis of the set of normalized patterns $\{\hat{\rho}_{mn}\}$. The functional tomogram displays a 3-dimensional map of the energy produced by all the sources located at a given point. To build a functional tomogram, the space under study is divided into $N_x \times N_y \times N_z$ elementary cubicles with centers in $\boldsymbol{r}_{ijs}$. The edge of the cubicle (spatial resolution) in this study was 1 mm. To calculate the energy produced by all the sources located in the center of the cubicle, the set of L trial magnetic dipoles $\boldsymbol{Q}_{ijsl}$ is build. The magnetic induction from the trial source can be derived from [24] for the coil with current I, radius a and direction $\boldsymbol{Q}_{ijsl}$, located in $\boldsymbol{r}_{ijs}$. For the sensor with location $\boldsymbol{r}_k$ and direction $\boldsymbol{n}_k$, the element of the trial pattern will be:

$$\rho^{tr}_{ijslk} = \frac{\mu_0 I}{\pi\alpha^2\beta}\left(\left(\frac{z}{d}\,(\alpha^2\,(E(\gamma^2) - K(\gamma^2)) - 2adE(\gamma^2))\boldsymbol{e_d} + (\alpha^2(K(\gamma^2) - E(\gamma^2)) + (2a^2 + 2ad)E(\gamma^2))\boldsymbol{Q_{ijsl}}\right), \boldsymbol{n_k}\right) \tag{8}$$

where:

$\alpha^2 = a^2 + d^2 + z^2 - 2da$; $\beta^2 = a^2 + d^2 + z^2 + 2da$; $\gamma^2 = 1 - \frac{\alpha^2}{\beta^2}$;

$\boldsymbol{r_a} = \boldsymbol{r_k} - \boldsymbol{r_{ijs}}$; $z = (\boldsymbol{r_a}, \boldsymbol{Q_{ijsl}})$; $\boldsymbol{d} = \boldsymbol{r_a} - z\boldsymbol{Q_{ijsl}}$; $d = |\boldsymbol{d}|$; $\boldsymbol{e_d} = \frac{\boldsymbol{d}}{|d|}$;

$|\boldsymbol{n_k}| = 1$;

$K(\gamma^2)$ – elliptic integral of the first kind, $E(\gamma^2)$ – elliptic integral of the second kind.

At each node of the grid $\boldsymbol{r}_{ijs}$, there are L directions of trial magnetic dipoles, uniformly covering the sphere, in this study $L = 931$. Then the set of normalized trial patterns is calculated:

$$\hat{\boldsymbol{\rho}}^{tr}_{ijsl}, \quad i = 1, ..., N_x;$$
$$j = 1, ..., N_y;\ s = 1, ..., N_z;\ l = 1, ..., L. \tag{9}$$

In this study, 931 million of trial patterns are used for the functional tomography of the experimental space $100 \times 100 \times 100$ cubic millimeters.

For each normalized experimental pattern in (7), $\hat{\boldsymbol{\rho}}_{mn}$, the following function is calculated, giving the difference between this pattern and one of the trial patterns:

$$\chi(i, j, s, l) = \sum_{k=1}^{K} (\hat{\rho}_{mnk} - \hat{\rho}^{tr}_{ijslk})^2 \tag{10}$$

The position and direction of the source producing the pattern $\hat{\boldsymbol{\rho}}_{mn}$ are determined by numbers (I, J, S, L) providing the minimum to the function $\chi(i, j, s, l)$ over the variables $i = 1, ..., N_x$; $j = 1, ..., N_y$; $s = 1, ..., N_z$; $l = 1, ..., L$.

The energy of this source D^2_{mn} is added to the energy produced from the cubicle with the center at $\boldsymbol{r}_{IJS}$.

Performing this procedure for all normalized experimental patterns: $m = 1, ..., M$; $n = 1, ..., N$, it is possible to distribute in space the energy of all oscillations from formula (7). The result of such distribution is the functional tomogram of the experimental space, reconstructed from multichannel magnetic recordings. Functional tomogram shows the spatial distribution of the energy, produced by the object under study.

Directional functional tomogram displays a 3-dimensional map of the vector field, produced by all the sources located at a given point. The direction of the vector at each node of the grid is a dominant direction of the L trial directions ($L = 931$ in this study). Fig. 2 illustrates the set of 931 trial directions and the dominant directions 457, 458, 459 corresponding to frequencies close to 5.8 Hz (see Fig. 3). The amplitude of the vector is proportional to the energy, generated in dominant direction. In this study each vector is represented as a colored stick. The middle point of the stick is located at the node of the grid, the stick itself shows the direction of oscillation, while the color represents the amplitude in correspondence with the Legend (Fig. 5d).

3. Results and discussion

3.1. Experimental detection of the spatial anisotropy of magnetic noise generated by the stationary standing vial with the ferrofluid

The synthesized ferrofluid was placed in a 40 ml plastic vial. The vial was placed on a nonmagnetic stand situated at 8 cm under the central gradiometer of the measuring head of the MEG device. MEG noise recordings were collected with the sample and without the sample. The duration of one recording was 20 min. Fourier transform of the signals from each SQUID channel was generated and directional functional tomogram was calculated by the method, proposed in Refs.

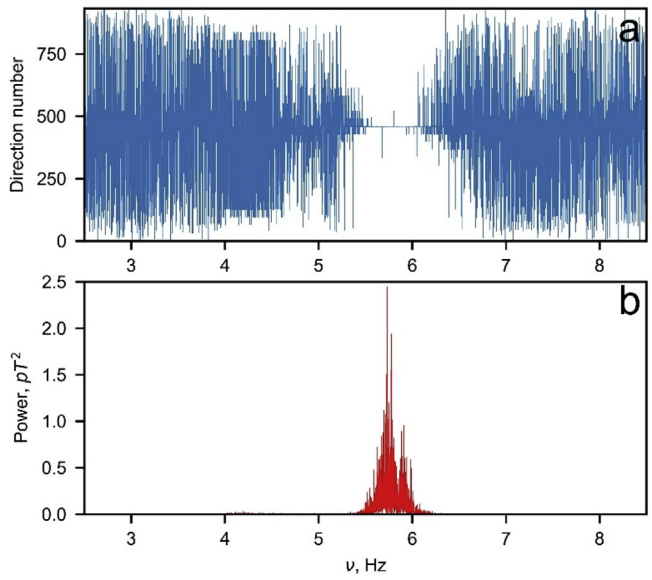

Fig. 3. a – Spatial angular distribution of the magnetic noise, generated by the vial with ferrofluid, as a function of the noise frequency; b – Power of the magnetic noise, generated by the vial, as a function of the noise frequency.

[19–21] and described in 2.4. Then the summary power in all channels was calculated (6).

In Fig. 3b it is shown that the insertion of the vial with ferrofluid into the MEG device increases the amplitude of the noise in the frequency band 5–6 Hz by two orders of magnitude.

In Fig. 3a the dependence of the spatial angular distribution of the magnetic noise, generated by the vial with ferrofluid, on the frequency of the noise is shown. Angular distribution of the noise was estimated from the direction number of the source found for each frequency. Total number of possible directions is 931 for each trial source. Broad angular distribution corresponds to noisy solutions with low power, generated presumably by magnetometer channels themselves. Narrow angular distributions correspond to magnetic fields, generated by the fluctuation of ferrofluid. The direction of this fluctuation can be estimated from the dominant directions of the sources, found from these distributions.

As can be concluded from Fig. 3, the magnetic sources oscillations, corresponding to the high-power solutions, are strongly anisotropic. The reason of this phenomena is anisotropy of the weak mechanical oscillations in experimental setup. The source of these infrasound oscillations is the urban environment of Moscow city. The observed effect makes it possible to reveal extra weak oscillations and to determine their directions.

3.2. Study of the dependence of the angular distribution of the noise generated by the vial on the viscosity of the ferrofluid

As we have demonstrated earlier [18], the waves on the free surface of a magnetic liquid in the vial generate the dominant noise signal. Such free liquid surface is absent in the living cell. Therefore the noise signal from the samples of gelatinized and frozen ferrofluid was investigated in order to evaluate the applicability of the proposed methodology to such living systems.

The vial with samples of ferrofluid was placed on a nonmagnetic stand situated at 8 cm under the peripheral gradiometer with a displacement of 3 cm from the center of the measuring head of the MEG device. MEG noise recordings were collected with the sample and without the sample. The duration of one recording was 20 min. Fourier transform of the signals from each SQUID channel was generated and directional functional tomogram was calculated by method, proposed in Refs. [19–21] and described in Section 2.4. Then the summary power in all channels was calculated (6).

In Fig. 4 the dependence of the spatial angular distribution of the magnetic noise, generated by the vial with ferrofluid, on the frequency of the noise is shown for various viscosities of ferrofluid. Angular distribution of the noise was estimated from the direction number of the source found for each frequency. Total number of possible directions is 931 for each trial source. Broad angular distribution corresponds to noisy solutions with low power, generated by magnetometer channels. Narrow angular distributions correspond to magnetic fields, generated by the fluctuation of ferrofluid. The direction of this fluctuation can be estimated from the dominant directions of the sources, found from these distributions.

It is found that in all experiments there are dominant directions for solutions in frequency band corresponding to power peak, thus confirming the effect, shown in Fig. 3. At the same time, details of angular

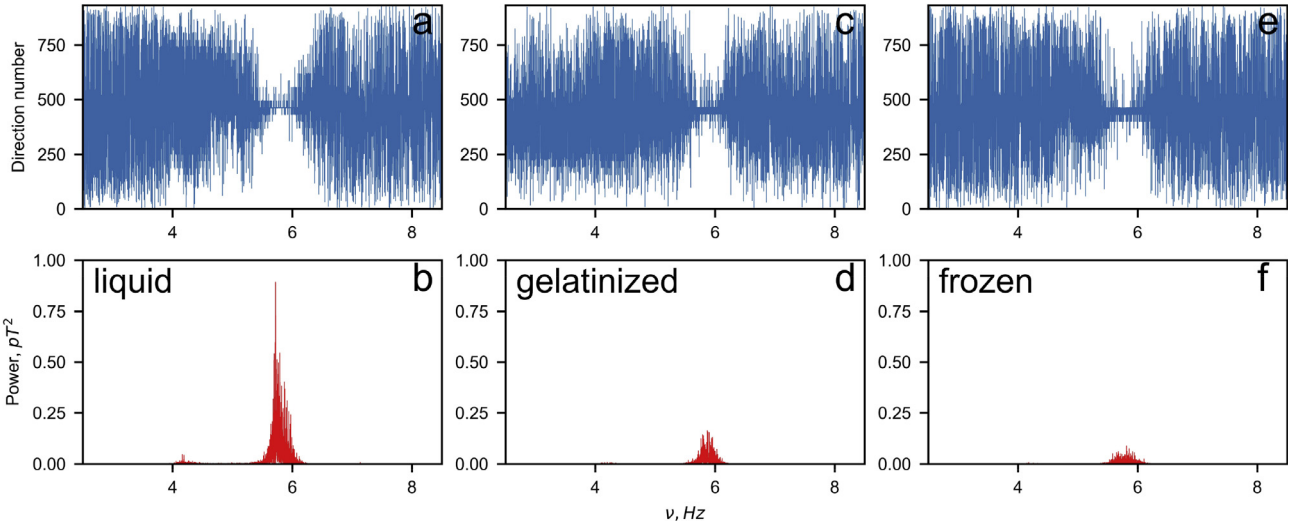

Fig. 4. a – Spatial angular distribution of the magnetic noise, generated by the vial with liquid ferrofluid, as a function of the noise frequency; b – Power of the magnetic noise, generated by the vial with liquid ferrofluid, as a function of the noise frequency; **c** – Spatial angular distribution of the magnetic noise, generated by the vial with gelatinized ferrofluid, as a function of the noise frequency; **d** – Power of the magnetic noise, generated by the vial with gelatinized ferrofluid, as a function of the noise frequency; **e** – Spatial angular distribution of the magnetic noise, generated by the vial with frozen ferrofluid, as a function of the noise frequency; **f** – Power of the magnetic noise, generated by the vial with frozen ferrofluid, as a function of the noise frequency;

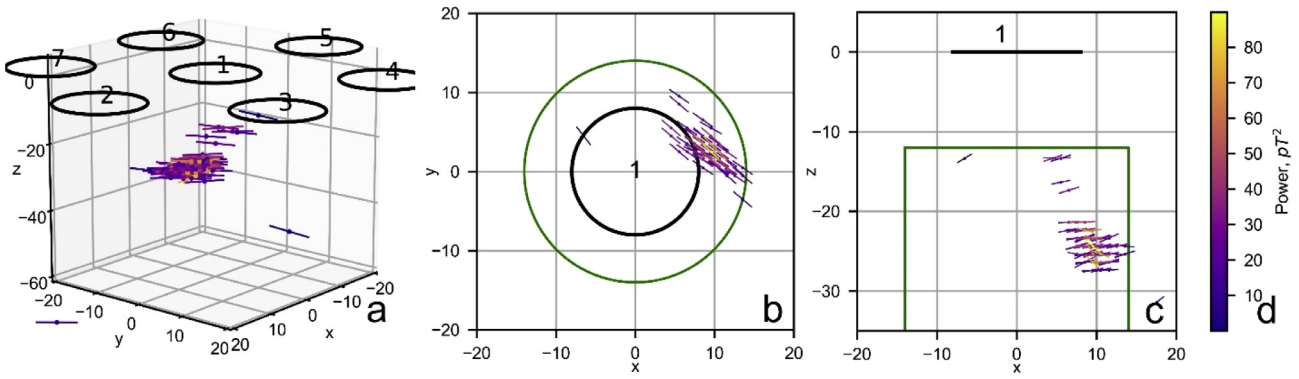

Fig. 5. a – 3D-view of the object (directional functional tomogram) and the measuring device (planar set of seven sensors); b – top view of the object; c – side view of the object; d – Legend for the source power presentation by the color. Green line is the vial contour. (For interpretation of the references to color in this figure legend, the reader is referred to the web version of this article.)

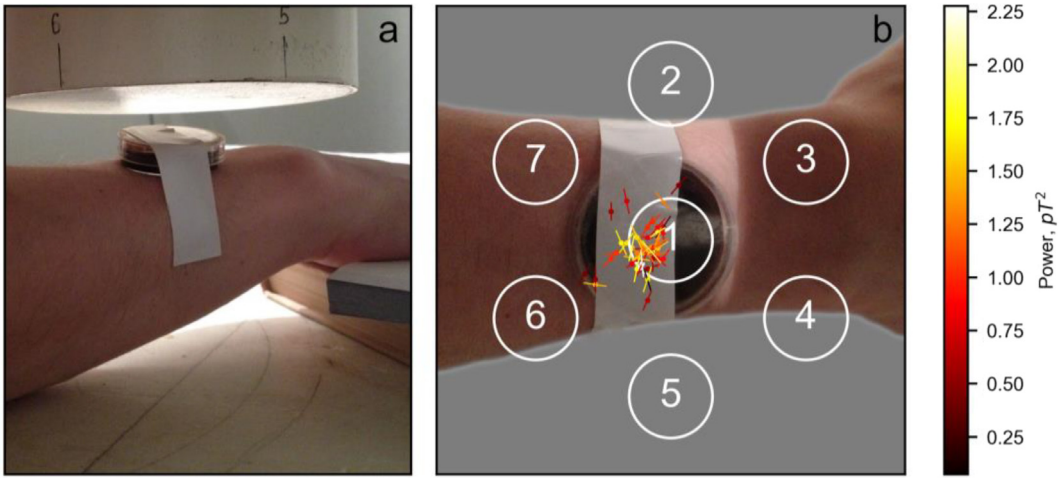

Fig. 6. a – General layout of the experiment, showing position of the hand with ferrofluid and the measuring device; b – top view of the object (directional functional tomogram in the frequency band 0.9–1.5 Hz) and the plot of the measuring device (planar set of seven sensors) combined with the hand photo. Also, the Legend is shown for the power presentation by color. (For interpretation of the references to colour in this figure legend, the reader is referred to the web version of this article.)

distributions differ for various viscosities. It can be concluded, that different inner movements of the ferrofluid are inherent for liquids with different viscosities and can be studied by the observed effect.

3.3. Localization of the vial with the ferrofluid by using the acoustic noise of our experimental setup and directions of magnetic sources

The vial with ferrofluid was installed under the central gradiometer of the measuring head of the MEG device. The free surface of the ferrofluid was situated at approximately 2 cm below the plane of the sensors. MEG noise recordings were collected for 20 min. Fourier transform of the signals from each SQUID channel was generated and directional functional tomogram was calculated by method, proposed in Refs. [19–21] and described in Section 2.4. Directional functional tomogram makes it possible to localize the magnetic sources and to represent their directions. In this study localization and directions are presented for the frequency band 5.3–6.3 Hz in a cube with a side of 100 mm, which is located under the device, with a resolution of 1 mm. Fig. 5 shows three views of the directional functional tomogram of the object. Also shown are the measuring device (the planar set of seven sensors), and the Legend.

Fig. 5 shows a directional functional tomogram of the object – set of sources, reconstructed from MEG recordings of magnetic noise. 3D-view of the vector field representing the position, direction and power of the sources confirms observations shown in Figs. 3 and 4 about the dominant direction of magnetic sources.

3.4. Localization of the vial with the ferrofluid by using a human heartbeat setup and directions of magnetic sources

The following experimental setup was used to study localization and directions of the sources in case of different ferrofluid oscillations. A Petri cap was partially filled with a ferrofluid and fixed on the hand as wristwatches. The hand was placed on the center of nonmagnetic stand situated at 3 cm under the measuring head of our 7-channel MEG device. MEG recordings were collected for 20 min.

Fourier transform of the signals from each SQUID channel was generated and directional functional tomogram was calculated by method, proposed in Refs. [19–21] and described in Section 2.4. In this study localization and directions are presented for the frequency band 0.9–1.5 Hz in a cube with a side of 100 mm, which is located under the device, with a resolution of 1 mm. Fig. 6 shows a directional functional tomogram of the object – set of sources, reconstructed from MEG recordings of magnetic fields, produced by the ferrofluid on the hand, in combination with the photo of the hand.

It is found that in this experiment the localization of the sources corresponds to the Petri cup position, but there is no dominant direction. The reasons for broad directions distribution can be the nature of ferrofluid waves in broad flat vial and the mechanical movement of the vial, produced by the hand, as in ballistocardiography [25]. It can be concluded, that different surface movements of the ferrofluid can be studied by the observed effect.

4. Conclusion

It was found, that the magnetic noise, generated by the stationary standing vial with the ferrofluid in geomagnetic field, have strong spatial anisotropy. Narrow angular distribution of generated magnetic signal corresponds to fluctuation movement of magnetic nanoparticles. The direction of these fluctuations can be estimated by the method [19–21] from the dominant direction of the sources, found from the angular distribution of the magnetic noise. The effect can essentially increase the spatial resolution of the proposed method of visualization of the distribution of superparamagnetic nanoparticles within a living organism [18]. In this method the natural fluctuation movement of living organism, caused by breath or heartbeat, leads to the movement of magnetic particles. The possibility of visualizing the directions of motion of nanoparticles will allow to establish an additional link with the physiology of the organs labeled by them.

Acknowledgments

Sections 2.1 and 2.2 were done by M.A. Polikarpov, A.Y. Yurenya, S.P. Naurzakov, A.P. Grebenkin and V.Y. Panchenko. Sections 2.3 and 2.4 were done by M.N. Ustinin and S.D. Rykunov. Sections 3.1–3.4 were done by M.A. Polikarpov, M.N. Ustinin, S.D. Rykunov, A.Y. Yurenya, S.P. Naurzakov, A.P. Grebenkin, V.Y. Panchenko. The work of M.A. Polikarpov, A.Y. Yurenya, S.P. Naurzakov and A.P. Grebenkin was partly supported by the Russian Foundation for Basic Research (grants 18-02-00629, 18-08-01349). The work of M.A. Polikarpov, A.Y. Yurenya, M.N. Ustinin and S.D. Rykunov was supported by the Russian Science Foundation (grant 18-11-00178).

References

[1] B. Gleich, J. Weizenecker, Tomographic imaging using the nonlinear response of magnetic particles, Nature 435 (2005) 1214–1217.
[2] Rad, et al., Quantification of superparamagnetic iron oxide (SPIO)-labeled cells using MRI, J. Magn. Reson. Imaging 26 (2) (2007) 366–374.
[3] A. Coene, et al., Multi-color magnetic nanoparticle imaging using magnetorelaxometry, Phys. Med. Biol. 62 (2017) 3139–3157.
[4] M.K. Kuimova, et al., Imaging intracellular viscosity of a single cell during photoinduced cell death, Nat. Chem. 1 (2009) 69–73.
[5] D. Cabrera, et al., Dynamical magnetic response of iron oxide nanoparticles inside live cells, ACS Nano (2018) 12, https://doi.org/10.1021/acsnano.7b08995.
[6] S. Moise, et al., The cellular magnetic response and biocompatibility of biogenic zinc- and cobalt-doped magnetite nanoparticles, Sci. Rep. 7 (2017) 39922.
[7] D. Soukup, et al., In situ measurement of magnetization relaxation of internalized nanoparticles in live cells, ACS Nano 9 (2015) 231–240.
[8] A.F. Davila, et al., A new model for a magnetoreceptor in homing pigeons based on interacting clusters of superparamagnetic magnetite, Phys. Chem. Earth 28 (2003) 647.
[9] M. Lévy, et al., Modeling magnetic nanoparticle dipole-dipole interactions inside living cells, Phys. Rev. B 84 (2011) 075480.
[10] M. Levy, et al., Nanomagnetism reveals the intracellular clustering of iron oxide nanoparticles in the organism, Nanoscale 3 (2011) 4402–4410.
[11] O. Laslett, et al., Interaction effects enhancing magnetic particle detection based on magneto-relaxometry, Appl. Phys. Lett. 106 (2015) 012407.
[12] Ling-Jun Kong, et al., In-vivo biomagnetic characterisation of the American cockroach, Sci. Rep. 8 (2018) 5140.
[13] D. Faivre, D. Schuler, Magnetotactic bacteria and magnetosomes, Chem. Rev. 108 (2008) 4875–4898.
[14] Davila, et al., Magnetic pulse affects a putative magnetoreceptor mechanism, Biophys. J. 89 (2005) 56–63.
[15] W. Jia, G. Xu, R.J. Sclabassi, J.G. Zhu, A. Bagic, M. Sun, Detection of magnetic nanoparticles with magnetoencephalography, J. Magn. Magn. Mater. 320 (2008) 1472–1478.
[16] T. Cheung, K. Kavanagh, U. Ribary, A new technique for magnetic nanoparticle imaging for magnetoencephalography using frequency data, Front. Neurosci. in: Conference Abstract: Biomag 2010 – Proceedings of the 17th International Conference on Biomagnetism, 2010, https://doi.org/10.3389/conf.fnins06.00387.
[17] J. Leliaert, et al., Thermal magnetic noise spectra of nanoparticle ensembles, Appl. Phys. Lett. 107 (2015) 222401, , https://doi.org/10.1063/1.4936890.
[18] M.A. Polikarpov, M.N. Ustinin, S.D. Rykunov, A.Y. Yurenya, S.P. Naurzakov, A.P. Grebenkin, V.Y. Panchenko, 3D imaging of magnetic particles using the 7-channel magnetoencephalography device without pre-magnetization or displacement of the sample, J. Magn. Magn. Mater. 427 (2017) 139–143, https://doi.org/10.1016/j.jmmm.2016.10.055.
[19] R.R. Llinás, M.N. Ustinin, Precise Frequency-Pattern Analysis to Decompose Complex Systems into Functionally Invariant Entities: U.S. Patent. US Patent App. Publ. 20160012011 A1. 01/14/2016.
[20] R.R. Llinás, M.N. Ustinin, Frequency-pattern functional tomography of magnetoencephalography data allows new approach to the study of human brain organization, Front. Neural Circuits 8 (2014) 43, https://doi.org/10.3389/fncir.2014.00043.
[21] R.R. Llinás, M.N. Ustinin, S.D. Rykunov, A.I. Boyko, V.V. Sychev, K.D. Walton, G.M. Rabello, J. Garcia, Reconstruction of human brain spontaneous activity based on frequency-pattern analysis of magnetoencephalography data, Front. Neurosci. 9 (2015) 373, https://doi.org/10.3389/fnins.2015.00373.
[22] Matteo Frigo, Steven G. Johnson, The design and implementation of FFTW3, Proc. IEEE 93 (2) (2005) 216–231 Invited paper, special issue on program generation, optimization, and platform adaptation.
[23] A. Belouchrani, K. Abed-Meraim, J.-F. Cardoso, E. Moulines, A blind source separation technique using second-order statistics, IEEE Trans. Signal Process. 45 (1997) 434–444, https://doi.org/10.1109/78.554307.
[24] M.W. Garrett, Calculation of fields, forces, and mutual inductances of current systems by elliptic integrals, J. Appl. Phys. 34 (9) (1963) 2567–2573, https://doi.org/10.1063/1.1729771.
[25] L. Giovangrandi, O. Inan, R. Wiard, M. Etemadi, G. Kovacs, Ballistocardiography – a method worth revisiting, Conf. Proc. IEEE Eng. Med. Biol. Soc. 2011 (2011) 4279–4282, https://doi.org/10.1109/IEMBS.2011.6091062.